Computational and experimental studies of convective fluid motion and heat transfer in inclined non-rectangular enclosures

T. S. Lee*

Computational and experimental studies of the fluid motion and heat transfer characteristics of an incompressible fluid contained in a non-rectangular inclined enclosure are described in this paper. The enclosure has two 45° inclined side walls one of which was heated and the other cooled. The remaining two sides of the enclosure are parallel and insulated. The enclosure was rotated about the long axis in steps of 30° through 360°. Experiments were performed to study the effects of Rayleigh number, aspect ratios and orientation of the enclosure. The computational method uses a mesh transformation technique coupled with the introduction of 'false transient' parameters for the steady state solution of the problem. The experimental method uses smoke for flow visualization studies. With aspect ratios of 3 and 6, the results indicate that the heat transfer and fluid motion within the enclosure is a strong function of both the Rayleigh number and the cavity orientation angle. A minimum and a maximum mean Nusselt number occurred as the angle of inclination was increased from 0 to 360°. A transition in the mode of circulation occurred at the angle corresponding to the minimum or maximum rate of heat transfer. Stream lines and isotherms are presented for the most representative cases

Key words: *Convection, fluid mechanics, inclined enclosures*

Steady two-dimensional buoyancy driven recirculating flows, particularly those in rectangular enclosures with isothermal but differentially heated vertical end walls and insulated horizontal walls, have been studied extensively during the past two decades. Catton[1] has reviewed the large body of work in this area prior to 1978. More recently, attention has been given to tilted rectangular enclosures[2–11]. Analytical studies for the stability of flow in inclined cavities have been performed by Hart[12] while experimental results are best represented by the work of Ozoe *et al*[13–15], Hollands and Koniceck[16], Wirtz, Righi and Zirilli[10] and Arnold, Catton and Edwards[17]. Catton, Ayyaswamy and Clever[18] presented some numerical calculations for $A=2$ and 5 and Wirtz and Tseng[11] presented two-dimensional finite difference solutions for $A=2$ and 5 for tilt angles ranging from $\phi=-90°$ (heating from above) to $\phi=+90°$ (heating from below). A three-dimensional numerical study of convection patterns in an inclined differentially heated box was carried out by Graham and Mallinson[19].

Numerical methods and flow visualization studies have been widely used for inclined rectangular enclosures. Little appears in the literature for the case of inclined non-rectangular cavities, the only obvious relevant work being that of Chung and Trefethen[4]. The purpose of this work was to study the flow behaviour and its effects on the heat transfer and temperature distribution within a non-rectangular enclosure. The non-rectangular enclosure chosen is of trapezoidal cross-section with two 45° inclined side walls one of which was heated and the other cooled. The remaining two sides of the enclosure are parallel and insulated (Fig 1). The parameters studied are for aspect ratios of 3 and 6 and Prandtl number of 0.7; Rayleigh number of the fluid is allowed to vary from 10^2 to 10^5 and the angle of tilt varied from 0° to 360° in steps of 30°. In the analysis, it is assumed that the fluid motion is two-dimensional and confined to the $x-y$ plane of Fig 1. The viscous effects due to the presence of end walls are neglected since Ozoe *et al*[14] have shown that if the width/length ratio is greater than 1, this effect is absent. Ozoe *et al* also showed that for high Rayleigh number there is a possibility of three-dimensional flow patterns when the enclosure is tilted above a critical angle. Above this critical angle, a stable roll mode of convection with its axis parallel to the z-axis might be expected. Therefore we expected that our two-dimensional numerical results would deviate from the experimental observation as the tilted angle approaches this critical angle. Outside this range, the convection should be two-dimensional and confined to the $x-y$ plane of Fig 1.

* Senior Lecturer, Mechanical and Production Engineering Department, Faculty of Engineering, National University of Singapore, Kent Ridge, Singapore 0511
Received 19 May 1983 and accepted for publication on 8 October 1983

 0142–727X/84/010029–08$03.00

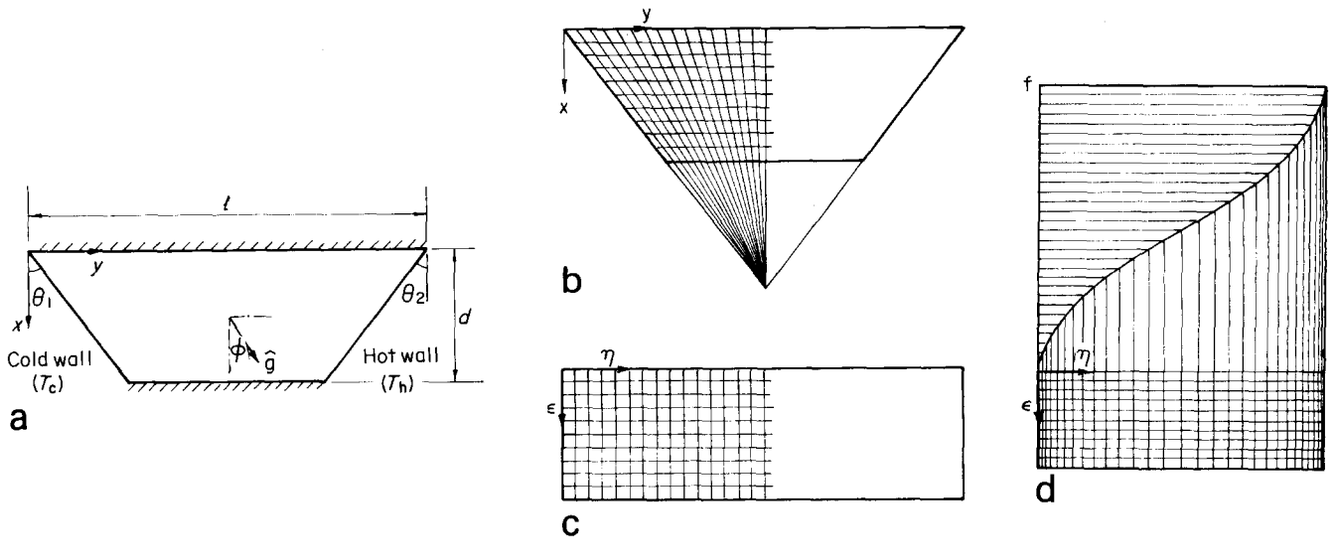

Fig 1 The model, its coordinates and mesh systems

Governing equations

If we restrict our attention to two-dimensional, steady laminar flow with constant properties, then the governing equations which describe the motion of the incompressible fluid in the inclined trapezoidal enclosure, subjected to Bousinesq approximation are: Momentum equations:

$$\frac{D\bar{u}}{Dt} = -\frac{\nabla p}{\rho_R} - \beta(T - T_R)\bar{g} + \nu\nabla^2\bar{u} \tag{1}$$

continuity equation:

$$\nabla \cdot \bar{u} = 0 \tag{2}$$

Energy transport equation:

$$\frac{DT}{Dt} = \alpha\nabla^2 T \tag{3}$$

Using the vector identity:

$$(\nabla \times \bar{u}) \times \bar{u} = \bar{u} \cdot \nabla\bar{u} - \nabla\overline{u^2}/2$$

taking curl of Eq (1), and invoking Eq (2), the resulting equation is:

$$\frac{\partial\bar{\zeta}}{\partial t} - \nabla \times (\bar{u} \times \bar{\zeta}) = -\beta\nabla \times (T - T_R)\bar{g} + \nu\nabla^2\bar{\zeta} \tag{4}$$

With the vorticity vector given by:

$$\bar{\zeta} = \nabla \times \bar{u} \tag{5}$$

Introducing the dimensionless variables

$$x^* = x/d \qquad y^* = y/l;$$

$$u^* = u/(\alpha/L) \qquad v^* = v/(\alpha/L);$$

$$\zeta^* = \zeta/(\alpha/L^2) \qquad \psi^* = \psi/\alpha;$$

$$\theta = (T - T_c)/(T_h - T_C) \qquad t = t/(L^2/\alpha);$$

where x^*, y^*, u^*, v^*, ζ^*, ψ^*, θ and t^* represent the dimensionless coordinates, velocities, vorticity, stream function, temperature and time respectively. The characteristic length L is defined as $(d \times l)^{1/2}$.

Notation

A	Aspect ratio (l/d)
d	Depth of cavity
g	Gravitational constant
l	Length of cavity
L	Characteristic length, $(lxd)^{1/2}$
M, N	mesh sizes
$\underline{Nu}$	Local Nusselt number
$\overline{Nu}$	Mean Nusselt number
Pr	Prandtl number, ν/α
P	Pressure
Ra	Rayleigh number, $\beta g L^3 \nabla T/\nu\alpha$
Δt	Time increment
T	Temperature
T_h, T_c	Temperature of hot and cold walls
u	Velocity in the x-direction
v	Velocity in the y-direction
x, y, z	Rectangular coordinates
∇^2	Laplace Operator
α	Thermal diffusivity
β	Thermal coefficient of volumetric expansion
ε	Dimensionless transformed x-coordinate
ζ	Vorticity
η	Dimensionless transformed y-coordinate
θ	Dimensionless temperature
θ_1, θ_2	Angles of slope of side walls
ν	Kinematic viscosity
ρ_0	Reference density
ϕ	Orientation angle of cavity
ψ	Stream function

With the above dimensionless variables, Eqs (3) and (4) become:

$$\frac{\partial\theta}{\partial t}+\bar{u}^*\cdot\nabla^2\theta=\nabla^2\theta \tag{6}$$

$$\frac{\partial\bar{\zeta}^*}{\partial t}-\nabla\times(\bar{u}^*\times\bar{\zeta}^*)=-RaPr(\nabla\times\theta\bar{g})+Pr(\nabla^2\bar{\zeta}^*) \tag{7}$$

where all variables are now in dimensionless form. With the vorticity vector defined by Eq (5), the stream function $\bar{\psi}$, is defined, such that a ψ-isoline is a streamline, ie:

$$\bar{u}^*=\nabla\times\bar{\psi}^* \tag{8}$$

Substituting Eq (8) into Eq (5) gives

$$\bar{\zeta}^*=\nabla\times(\nabla\times\bar{\psi}^*) \tag{9}$$

and, since $\bar{\psi}$ requires to be solenoidal, hence:

$$\nabla\cdot\bar{\psi}^*=0 \tag{10}$$

It can be shown that Eq (9) can be written as a vector Poisson equation:

$$\bar{\zeta}^*=-\nabla^2\bar{\psi}^* \tag{11}$$

Steady state solution of Eqs (6), (7) and (11) may be solved by some iterative procedure, such as the Jacobi iteration, or by some relaxation methods[16]. If this approach is used, then for each overall iteration loop of the set of steady state equations ($\partial/\partial t=0$), there will be as many inner iteration loops as there are equations. Each of these inner iteration loops has to converge before the next overall iteration loop can be performed. For the set of steady state Eqs (6), (7) and (11), this procedure can become very time consuming. An improved method is to approach the steady state solution through the corresponding unsteady equations:

$$\frac{\partial\theta}{\partial t^*}+\bar{u}^*\cdot\nabla\theta=\nabla^2\theta \tag{12}$$

$$\frac{\partial\bar{\zeta}^*}{\partial t^*}-\nabla\times(\bar{u}^*\times\bar{\zeta}^*)=-RaPr(\nabla\times\theta\bar{g})+Pr(\nabla^2\bar{\zeta}^*) \tag{13}$$

where t^* is the dimensionless time.

This time-dependent transient approach to the steady state solution is attractive. If there is more than one equation of the vorticity-transport type, then most of the inner iteration loops are eliminated. Unfortunately, Eq (11) remains elliptic in form. Its numerical solution requires an iterative technique at each time step to determine the stream function at that time. The overall solution process is then multi-iterative.

For problems considered here, we are only interested in the steady state solutions. The inner iteration loop of stream function-vorticity equation $\zeta=-\nabla^2\bar{\psi}^*$ seems an unnecessary burden in terms of computing effort. If the steady state solution is unique, and is independent of the transient approach to it, then the steady state solution of Eqs (8)–(11) can be reached by introducing a transient term into the stream function-vorticity equation and treating the stream function as a transport quantity:

$$\frac{\partial\bar{\psi}^*}{\partial t^*}=\nabla^2\bar{\psi}^*+\bar{\zeta}^* \tag{14}$$

Numerical experimentation shows that the stability characteristics of Eqs (12), (13) and (14) varied according to the relative magnitudes of the source term in the respective equations, and that convective stability of the flow does not affect Eq (14). In terms of numerical stability with a fixed time increment Δt and fixed mesh sizes, Eq (14) was found to be the most stable, and the vorticity transport equation Eq (13) is numerically most unstable. Hence, some 'false transient' terms are introduced into Eq (14) to 'speed up' the solution and into Eq (13) to stabilize the solution for a fixed time increment. The steady state solution is finally obtained through a set of 'fast and stable' transient equations:

$$\frac{1}{\alpha_\psi}\frac{\partial\bar{\psi}^*}{\partial t^*}=\nabla^2\bar{\psi}^*+\bar{\zeta}^* \tag{15}$$

$$\frac{\partial\theta}{\partial t^*}+\bar{u}^*\cdot\nabla\theta=\nabla^2\theta \tag{16}$$

$$\frac{1}{\alpha_\zeta}\frac{\partial\bar{\zeta}^*}{\partial t^*}-\nabla\times(\bar{u}^*\times\bar{\zeta}^*)=-RaPr(\nabla\times\theta\bar{g})+Pr(\nabla^2\bar{\zeta}^*) \tag{17}$$

The values of α_ψ lies between 1.0 and 10, and the values of α_ζ lies between 0 and 1.0. The time-steps used in the numerical solution follow the Courant–Ferderic–Lewis conditions. For two dimensional problems in rectangular coordinates, Eqs (15)–(17) may be written as:

$$\frac{1}{\alpha_\zeta}\frac{\partial\zeta^*}{\partial t^*}+C_1u^*\frac{\partial\zeta^*}{\partial x^*}+C_2v^*\frac{\partial\zeta^*}{\partial y^*}=Pr\left(C_3\frac{\partial^2\zeta^*}{\partial x^*}+C_4\frac{\partial^2\zeta^*}{\partial y^*}\right)+C_5\frac{\partial T^*}{\partial x^*}+C_6\frac{\partial T^*}{\partial y^*} \tag{18}$$

$$\frac{\partial T^*}{\partial t^*}+C_1u^*\frac{\partial T^*}{\partial x^*}+C_2v^*\frac{\partial T^*}{\partial y^*}=C_3\frac{\partial^2T^*}{\partial x^{*2}}+C_4\frac{\partial^2T^*}{\partial y^*{}_2} \tag{19}$$

$$\frac{1}{\alpha_\psi}\frac{\partial\psi^*}{\partial t^*}=C_3\frac{\partial^2\psi^*}{\partial x^{*2}}+C_4\frac{\partial^2\psi^*}{\partial y^{*2}}+\zeta^* \tag{20}$$

where $C_1=L/d$, $C_2=L/l$, $C_3=C_1^2$, $C_4=C_2^2$, $C_5=-RaPrC_1\sin\alpha$, $C_6=RaPrC_2\cos\alpha$ and $L=(dxl)^{1/2}$. Velocities, given by a stream function ψ, in dimensionless form are:

$$u^*=C_2\frac{\partial\psi^*}{\partial y^*}\qquad v^*=-C_1\frac{\partial\psi^*}{\partial x^*} \tag{21}$$

For the rest of this paper the * for dimensionless quantities has been dropped for simplicity.

Governing equations in transformed space

Fig 1(a) shows the coordinate system of the inclined trapezoidal enclosure with side-slope θ_1 and θ_2. The inclination of the enclosure is defined by the tilted angle ϕ. The original space (Fig 1(b)) is transformed into the rectangular domain as shown in Fig 1(c) by introducing new coordinates:

$$\varepsilon=ax \quad \text{for} \quad 0\leq x\leq 1$$

$$\eta=b\frac{[y-F_1(x)]}{[F_2(x)-F_1(x)]} \quad \text{for} \quad 0\leq y\leq 1 \tag{22}$$

where a, b are scaling factors, chosen such that $0 \leq \varepsilon \leq 1$ for $0 \leq x \leq 1$ and $0 \leq \eta \leq 1$ for $0 \leq y \leq 1$. Functions $F_1(x)$ and $F_2(x)$ described the left- and right-hand boundary of the enclosure (these may be any analytical function or even tabular values). The transformation given above is satisfactory provided $|F_2(x) - F_1(x)| > 0$.

By replacing all the partial derivatives in Eqs (18)–(21) with partial derivatives with respect to the transformed variable, the equations become:

$$\frac{1}{\alpha_\zeta}\frac{\partial \zeta}{\partial t} + D_1 u\frac{\partial \zeta}{\partial \varepsilon} + (D_2 u + D_3 v + D_4)\frac{\partial \zeta}{\partial \eta} = D_5\frac{\partial^2 \zeta}{\partial \varepsilon^2} + D_6\frac{\partial^2 \zeta}{\partial \varepsilon\,\partial \eta} + D_7\frac{\partial^2 \zeta}{\partial \eta^2} + D_8\frac{\partial T}{\partial \eta} + D_9\frac{\partial T}{\partial \varepsilon} \tag{23}$$

$$\frac{\partial T}{\partial t} + E_1 u\frac{\partial T}{\partial \varepsilon} + (E_2 u + E_3 v + E_4)\frac{\partial T}{\partial \eta} = E_5\frac{\partial^2 T}{\partial \varepsilon^2} + E_6\frac{\partial^2 T}{\partial \varepsilon\,\partial \eta} + E_7\frac{\partial^2 T}{\partial \eta^2} \tag{24}$$

$$\frac{1}{\alpha_\psi}\frac{\partial \psi}{\partial t} + B_1\frac{\partial \psi}{\partial \eta} = B_2\frac{\partial^2 \psi}{\partial \varepsilon^2} + B_3\frac{\partial^2 \psi}{\partial \varepsilon\,\partial \eta} + B_4\frac{\partial^2 \psi}{\partial \eta^2} + \zeta \tag{25}$$

and the corresponding velocities are:

$$u = A_1\frac{\partial \psi}{\partial \eta} \qquad v = -\left(A_2\frac{\partial \psi}{\partial \varepsilon} + A_3\frac{\partial \psi}{\partial \eta}\right) \tag{26}$$

where A's, B's, D's and E's are constants resulting from the transformation and non-dimensionalization.

Boundary conditions

ψ at the boundaries are constant as there is no flow across the boundaries, ie $\psi = 0$ on the boundaries. Assuming no slip at the solid boundaries, thus $u = v = 0$. θ at the boundaries is given by:

$$\begin{aligned} &\theta = 0 \text{ along the cold wall } (\eta = 0)\\ &\theta = 1 \text{ along the hot wall } (\eta = 1)\\ &\frac{\partial \theta}{\partial x} = 0 \text{ along the adiabatic wall } (\varepsilon = 0 \text{ and } 1) \end{aligned} \tag{27}$$

Along the solid walls, the vorticity is evaluated from

$$\zeta = -\left(C_1^2\frac{\partial^2 \psi}{\partial x^2} + C_2^2\frac{\partial^2 \psi}{\partial y^2}\right) \tag{28}$$

Numerical methods

The solution region in Fig 1(b) is stretched into a rectangular domain as shown in Fig 1(c). This rectangular domain is then overlayed with a regular finite difference mesh. At the node points, the finite difference solutions to Eqs (18)–(21), with their boundary conditions, are obtained. The numerical procedure used involves an ADI method originally proposed by Peaceman and Rachford[20] and modified by Samarkii and Andreev[21]. For the vorticity transport equation, the advancement over one time step is accomplished through:

$$\begin{aligned} &[I - \sigma\,\Delta t A_\varepsilon](\zeta^*) = [A_\varepsilon + A_\eta](\zeta)^n + (S_D)^n\\ &[I - \sigma\,\Delta t A_\eta](\zeta)^{**} = (\zeta)^*\\ &(\zeta)^{n+1} = (\zeta)^n + \Delta t(\zeta)^{**} \end{aligned} \tag{29}$$

where $(\zeta)^*$ and $(\zeta)^{**}$ are dummy variables; A_ε and A_η are matrix operators formed through finite differencing of the governing equations in the ε and ζ directions respectively; $(S_D)^n$ is the source term evaluated at the most recent solution field; σ is a weighted time-step factor; I is an identity matrix. This scheme is equivalent to:

$$\begin{aligned} \frac{(\zeta)^{n+1} - (\zeta)^n}{\Delta t} = {} & (A_\varepsilon + A_\eta)(1-\sigma)(\zeta)^n\\ & + (A_\varepsilon + A_\eta)\sigma(\zeta)^{n+1}\\ & - \sigma^2\Delta t(A_\varepsilon A_\eta)((\zeta)^{n+1} - (\zeta)^n)\\ & + (S_D)^n \end{aligned} \tag{30}$$

For $\sigma = \frac{1}{2}$, the above scheme corresponds to the Crank–Nicholson equation.

The same method is adopted in solving the temperature and stream function-vorticity equations. All spatial derivatives are approximated by second-order-accurate centre differences. The convective terms in Eqs (18) and (19) are approximated by using a second order up-wind differencing method. The mixed spatial derivatives resulting from the mesh transformation are handled by the method proposed by McKee and Mitchell[22]. The resulting linear set of finite difference equations is then solved by an algorithm due to Thomas[23]. Three-point backward and forward difference formula are used for derivatives at the boundaries. The boundary vorticity values are obtained by considering the Taylor series expansion of ψ into the solution region and taking into consideration the ψ and the velocity at the boundary, ie along the parallel wall:

$$\zeta_w = -\frac{3C_n}{(\Delta\varepsilon)^2}(\psi_{w+1} - \psi_w) - \tfrac{1}{2}\zeta_{w+1}$$

and along the inclined wall:

$$\zeta_w = -\frac{3C'_n}{(\Delta\eta)^2}(\psi_{w+1} - \psi_w) - \tfrac{1}{2}\zeta_{w+1}$$

where C_n, C'_n are spatial constants resulting from transformation. Subscripts w and $w+1$ refer to the wall and the adjacent internal mesh point value respectively. Similar expressions were proposed by Wood[23].

Heat transfer at the inclined surfaces is defined by the local Nusselt number:

$$Nu = -\frac{\partial \theta}{\partial n}$$

where n is normal to the surface. Finer Nu was obtained with the non-uniform mesh generator as shown in Fig 1(d) where $f = 2/\pi \sin^{-1}(\eta^{1/2})$. The mean Nusselt number is then determined from:

$$\overline{Nu} = \int_0^1 Nu\,d\varepsilon$$

The mean Nusselt number is also used as the quantity to indicate steady state convergence. The mean Nusselt number is computed at every twentieth iteration. The steady state criteria is said to have satisfied when a difference of less than 0.1% of a reference Nusselt number ($Nu_{ref} = 1.0$) is detected. The computation of the Nusselt number requires the differentiation of the temperature function, and should therefore converge at a slower rate than the latter. This has proven satisfactory. The stream function, velocity, temperature and vorticity fields are noted to be steady when the Nusselt number is steady.

Experimental flow visualization technique

The apparatus used for the experimental model (Fig 2) was essentially similar to that described by Linthorst, Schinkel and Hoogendoorn[5], except for the trapezoidal cavity. The isothermal walls consist of brass-plate water jackets that were fed from constant temperature baths. The frame between the jackets was constructed from perspex with dummy cavities adjacent to the boundaries. The device has proved to be successful in ensuring that the parallel boundaries are adiabatic. The other boundaries were insulated by blocks of polystyrene foam. The cavity was mounted on a precision dividing head so that the cavity could be inclined at any required angle to within ±0.5°. The water in each jacket was maintained at a steady temperature to an accuracy of ±0.1 °C. The spatial variations of temperature within the jackets were measured by thermocouples immersed in the water. The flow rate of the water was adjusted to ensure that the variations were within ±0.1 °C.

The fluid motion was made visible by introducing a small quantity of cigarette smoke through long small diameter copper tube vents in the boundaries. The smoke was illuminated by a collimated beam of light to make observations in a particular plane of interest.

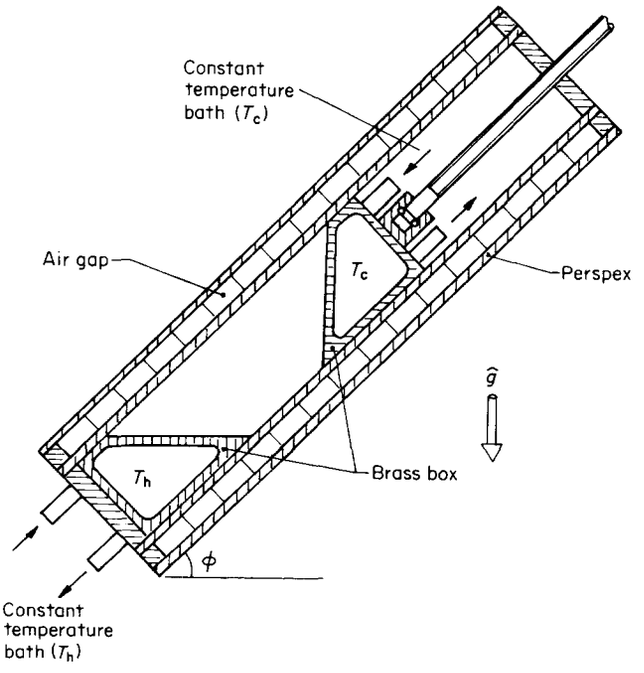

Fig 2 Experimental enclosure

After allowing several hours for the apparatus to reach thermal equilibrium, the smoke was introduced and the vents closed. It was found that the injected cigarette smoke circulated in the enclosure for about 15 minutes before it showed any signs of settling out on the walls. This confirmed the belief that cigarette smoke acts as if it were neutrally buoyant in air. The injection temperature did not necessarily match the local temperature within the enclosure. However, by the time a photograph was taken, the smoke had travelled around the enclosure a few times and should have come to equilibrium with the enclosed air.

Results and discussion

The discussion here is based on the steady state results obtained from the transient solutions of the governing equations with initial values of ψ, u, v, θ and ζ all set to zero, except the temperature at the cold and hot walls. The temperature θ is 0.0 at the cold wall and 1.0 at the hot wall. The mesh size used for the solutions illustrated here is 21×61.

For a low aspect ratio cavity ($A = 3.0$), the effects of variation of tilt angle on the temperature and streamline contours for $Ra = 10^3$ and 10^5 are shown in Fig 3. A study of the many corresponding

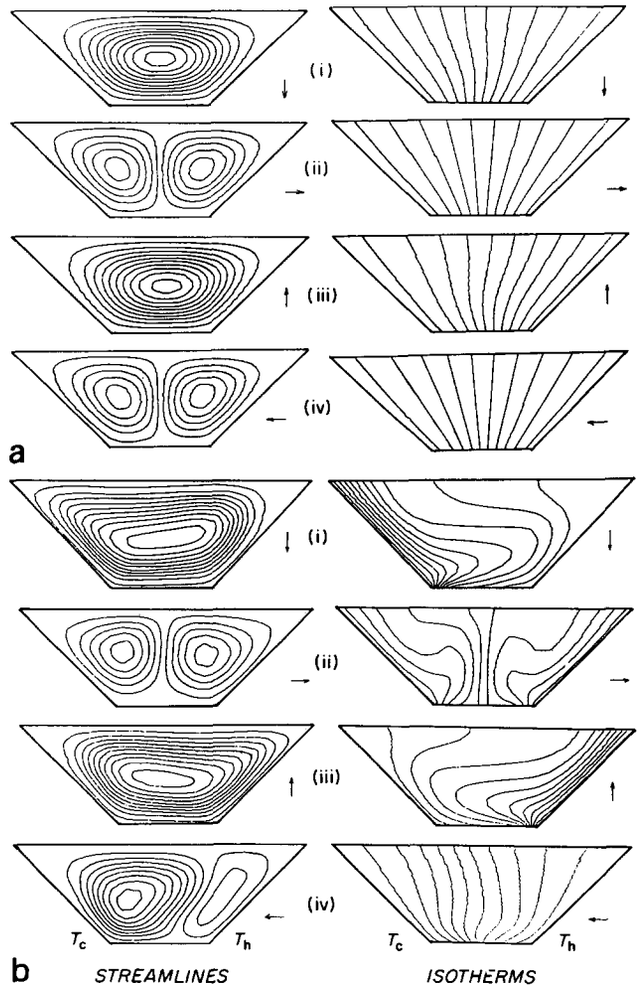

Fig 3 Numerical flow visualization for A = *3.0,* Pr = *0.7 with (a)* Ra = 10^3, *(b)* Ra = 10^5 *at* $\phi = 0°$, *90°, 180° and 270°*

runs that were made indicate that for $Ra = 10^2$ and 10^3 (Fig 3(a)) the conduction regime dominates, and transits at $Ra = 10^4$ before developing into strong boundary layer type of flow at $Ra = 10^5$ (Fig 3(b)). For the trapezoidal enclosure in the horizontal position, Figs 3(a)(i) and (b)(i) show that when the Ra is increased, the temperature and streamline contours become skewed. At $Ra = 10^5$, the flow although remaining uni-cellular, has skewed to the hot side due to the stronger convective current along the hot inclined wall. When the cavity is tilted until the hot wall is directly below the cold wall (Figs 3(a)(ii) and (b)(ii)), the flow pattern changes to a two-cell 'cat-eye' pattern, with one cell on top of the other. As Ra increases to 10^5, the temperature contours show a marked departure from the conduction pattern of $Ra = 10^3$. With the cavity inverted (Figs 3(a)(iii) and (b)(iii)), the flow patterns are similar to those in Figs 3(a)(i) and (b)(i), except that here the rising fluid along the inclined hot wall has a shorter path to the cold wall for the dissipation of heat. This was also indicated by the study of the mean Nusselt number, $\overline{Nu}$, which has a maximum value at this angle of tilt (Fig 6(a)). With the heated inclined wall at the top, the vertical temperature gradient is adverse to the buoyancy-induced flow, the fluid is therefore relatively stagnant and the temperature contours are characteristic of conduction. The situation is, however, slightly different from the corresponding case for a rectangular cavity. The cavity although heated at the top, is able to induce some fluid motion because of the inclination of the hot wall. Fluid heated at the bottom of the hot wall rises alongside the hot wall to the top, thus creating a weak convective cell near the top. This has also shown up in the mean Nusselt number study which show a minimum $\overline{Nu}$ at this angle of tilt (Fig 6(a)).

Flow visualization experiments were performed to verify the above flow pattern predicted by the finite difference study. Fig 4 shows the corresponding cases for $Ra \approx 2.0 \times 10^5$. The computed streamline is encouragingly similar to the smoke pattern. Fig 4(a) shows that at $\phi = 0$, the air close to the hot wall is heated and rises along the inclined wall. Cold air from the bottom replaces the rising hot air, thus creating a uni-cellular flow pattern. Similar flow patterns were observed for $\phi = 180°$ (Fig 4(c)). The uni-cellular flows in these cases are skewed towards the hot wall. For $\phi = 90°$ and $\phi = 270°$, Figs 4(b) and (d) show two counter-rotating cells, one near the hot wall and one near the cold wall. For $\phi = 270°$, however, the smoke does not show the two counter-rotating cells well due to the very stagnant nature of the flow under this condition.

When the aspect ratio is increased to 6.0, the corresponding streamline and temperature contour are shown in Fig. 5. The general trend is similar to that of Fig 3 except that now the temperature contours are more widely spaced and hence there is a general reduction in the mean Nusselt number for the corresponding cases. The corresponding mean Nusselt number versus angle of tilt for $A = 3.0$ and $A = 6.0$ is shown in Fig 6. The results indicate a maximum mean Nusselt number, $\overline{Nu}$, at around $\phi = 180°$ and minimum $\overline{Nu}$ at around $\phi = 270°$, irrespective of the Rayleigh number, for $A = 3.0$ and 6.0.

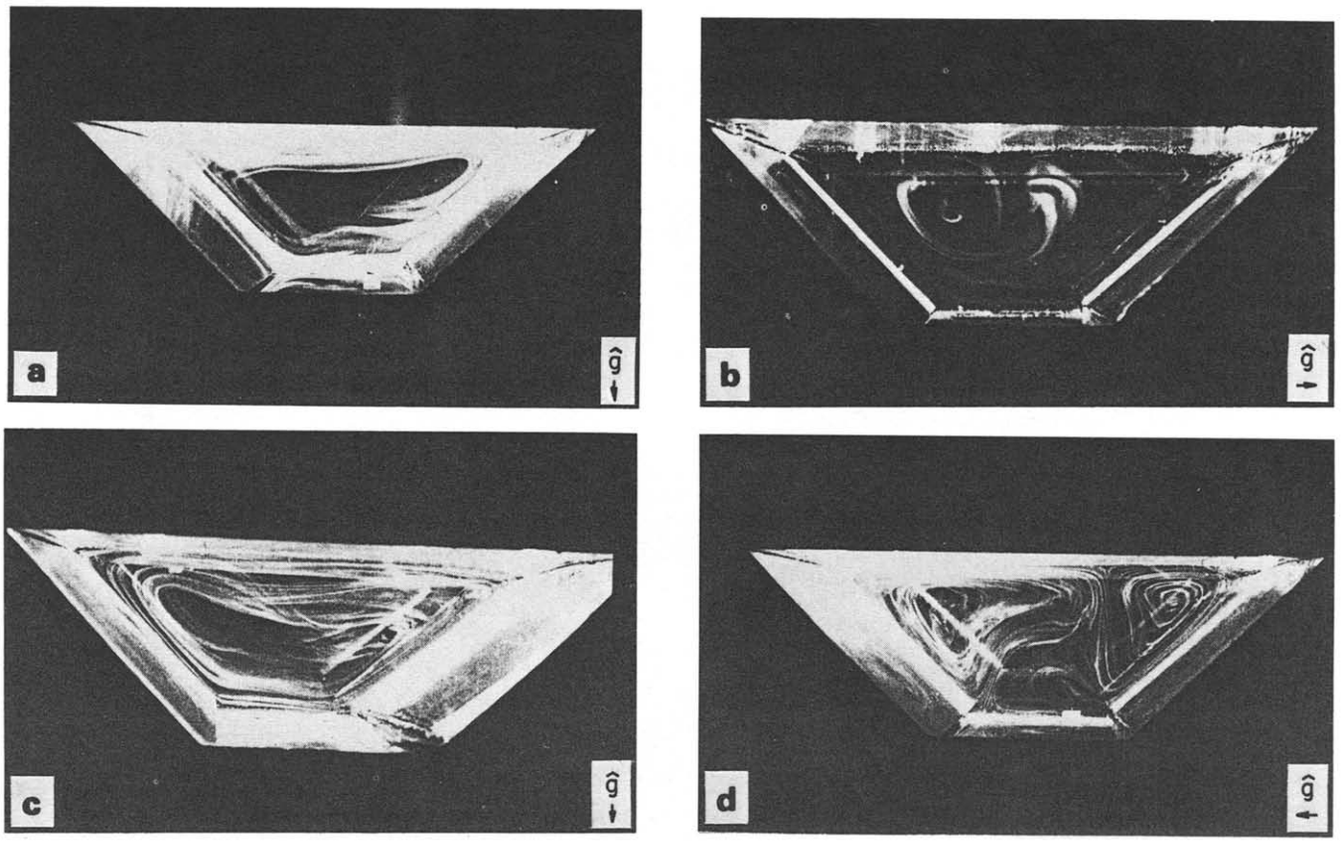

Fig 4 Experimental flow visualization for A = *3.0,* Pr = *0.7 (air) with* Ra $\approx 2 \times 10^5$ *at* $\phi = 0°$, *90°, 180° and 270°*

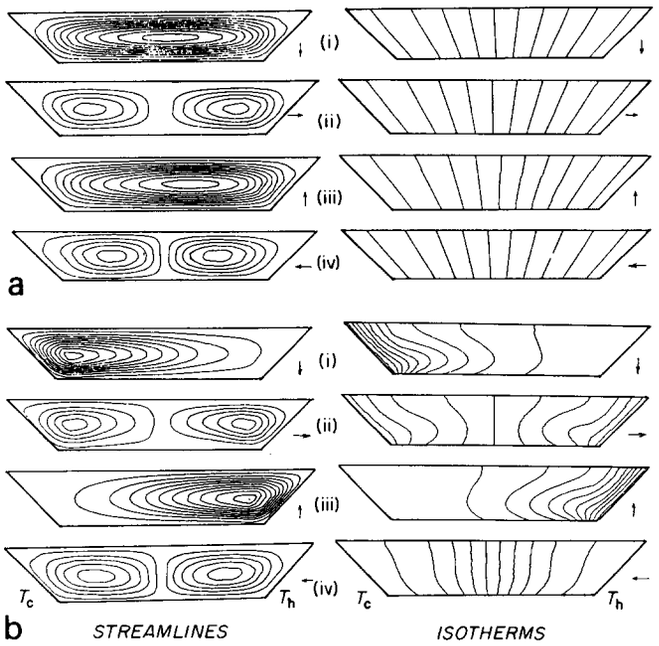

Fig 5 Numerical flow visualization for A = *6.0,* Pr = *0.7 with (a)* Ra = 10^3, *(b)* Ra = 10^5 *at* $\phi = 0°$, *90°, 180° and 270°*

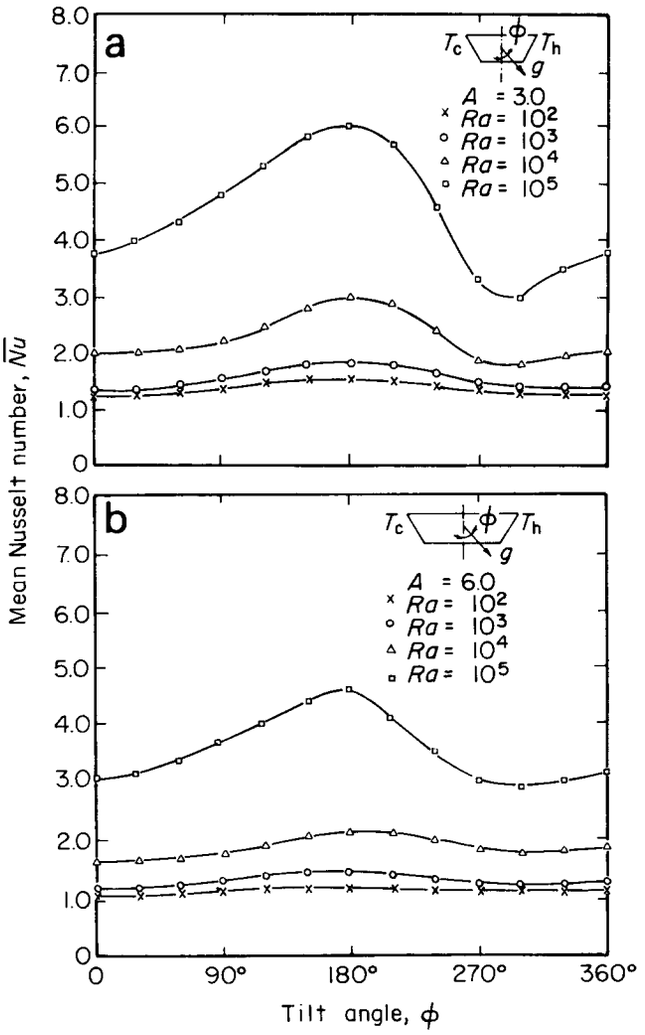

Fig 6 Variation of mean Nusselt number with tilt angle and Rayleigh number at aspect ratios of (a) A = *3.0 and (b)* A = *6.0*

Conclusion

The results presented here show that the heat transfer, in a trapezoidal enclosure with two 45° inclined side walls of moderate aspect ratios, is a strong function of the orientation angle of the cavity for *Ra* greater than 10^4. A maximum $\overline{Nu}$ occurs at around $\phi = 180°$ and minimum $\overline{Nu}$ occurs at around $\phi = 270°$, irrespective of the Rayleigh number. A transition in the mode of circulation within the enclosure occurred at the angle corresponding to the maximum or minimum $\overline{Nu}$. The mode of all flow patterns was verified from the finite difference solutions and the flow visualization experiment.

Acknowledgements

The author gratefully acknowledges the financial support of a National University of Singapore Research Grant (No RT21/82) and the assistance of K. S. Han and C. S. Tan during the course of this project.

References

1. **Catton I.** Natural Convection in Enclosures. *Procceedings of 6th International Heat Transfer Conference, Toronto, 1978, Vol. 6, Hemisphere Press, Washington, D.C., pp. 13–31*
2. **Bejan A. and Tien C. L.** Laminar natural convection heat transfer in a horizontal cavity with different end temperatures. *ASME J. Heat Transfer, 1978,* **100**, *641–647*
3. **Elsheribiny S. M., Hollands K. G. T. and Raithby G. D.** Effect of thermal boundary conditions on natural convection in vertical and inclined air layers. *ASME J. Heat Transfer, Aug 1982,* **104**, *515–520*
4. **Kyung Cho Chung and Lloyd M. Trefethen.** Natural convection in vertical stack of inclined parallelogrammic cavities. *Int. J. Heat Mass Transfer, 1982,* **25**, *No. 2, 277–284*
5. **Linthorst S. J. M., Schinkel W. M. M. and Hoogendoon C. J.** Flow structure with natural convection in inclined air-filled enclosures. *ASME J. Heat Transfer, Aug 1981,* **103**, *535–539*
6. **Meyer B. A., Mitchell J. W. and El-Wakil M. M.** The effect of thermal wall properties on natural convection in inclined rectangular cells. *ASME J. Heat Transfer, Feb 1982,* **104**, *111–117*
7. **Ozoe H., Chao P. K. B., Churchille S. W. and Lior N.** Laminar natural convection in an inclined rectangular box with the lower surface half heated and half insulated. *ASME J. Heat Transfer, 1982,* **104**, *1–7*
8. **Sernas V. and Lee E. I.** Heat transfer in an enclosure of aspect ratio less than one. *ASME J. Heat Transfer, November 1981,* **103**, *617–622*
9. **Strada M. and Heinrich J. C.** Heat transfer rates in natural convection at high Rayleigh number in rectangular enclosures: A Numerical Study. *Numerical Heat Transfer, 1982,* **5**, *81–93*
10. **Wirtz R. A., Righi J. and Zirilli F.** Measurements of natural convection across tilted rectangular enclosures of aspect ratio 0.1 and 0.2. *ASME J. Heat Transfer, Aug 1982,* **104**, *521–526*
11. **Wirtz R. A. and Tseng W. F.** Natural convection across tilted, rectangular enclosures of small aspect ratio. *19th National Heat Transfer Conference, Orlando, Florida, USA. HTD. Vol 78, 80-65786. July, 1980*

12. **Hart J. E.** Stability of the flow in a differentially heated inclined box. *J. Fluid Mech., 1971,* **47**, *547–576*

13. **Ozoe H., Sayama H. and Churchill S. W.** Natural convection in an inclined square channel. *Int. J. Heat & Mass Transfer, 1974,* **17**, *401–406*

14. **Ozoe H. and Sayama H.** Natural convection in an inclined rectangular channel at various aspect ratios and angles—experimental measurements. *Int. J. Heat & Mass Transfer, 1975,* **18**, *1425–1431*

15. **Ozoe H., Yamamoto K., Sayama H. and Churchill S. W.** Natural circulation in an inclined rectangular channel heated on one side and cooled on the opposing side. *Int. J. Heat & Mass Transfer, 1974,* **17**, *1209–1217*

16. **Hollands K. G. T. and Koniceck L.** Experimental study of the stability of differentially heated inclined air layers. *Int. J. Heat & Mass Transfer, 1973,* **16**, *1467–1476*

17. **Arnold J. N., Catton I. and Edwards D. K.** Experimental investigation of natural convection in inclined rectangular regions of differing aspect ratios. *J. Heat Transfer, 1976,* **98**, *66–71*

18. **Catton I., Ayyaswamy P. S. and Clever R. M.** Natural convection in an inclined square channel. *Int. J. Heat & Mass Transfer, 1974,* **17**, *173–184*

19. **Graham A. D. and Mallinson G. D.** Three-dimensional convection in an inclined differentially heated box. *6th Australasian Hydraulics and Fluid Mechanics Conference, Adelaide, Australia, 5–9 December, 1977*

20. **Peacemen D. W. and Rachford H. H. O.** The numerical solution of parabolic and elliptic differential equations. *J. SIAM, 1955,* **3**, *28–47*

21. **Samarskii A. A. and Andree V. B.** On a high accuracy difference scheme for an elliptic equation with several space variables. *U.S.S.R. Comp. Math. Math. Phys., 1963,* **3**, *1373–1382*

22. **McKees S. and Michell A. R.** Alternating direction methods for parabolic equations in two space dimensions with mixed derivatives. *The Computer Journal, 1970,* **13**, *No. 1, 81–86*

23. See **Roach P. J.** Computational Fluid Dynamics. *Hermosa Publishers, Albuquerque, New Mexico, 1973*

24. **Cheng K. C. and Ou J. W.** Buoyancy and tilt angle effects on Graetz problem in horizontal rectangular channels. *ASME/JSME Thermal Engineering Joint Conference, Honolulu. Proceedings Vol. 3, p. 141–147, 1983*

BOOK REVIEW

Photon Correlation Techniques in Fluid Mechanics

Ed. E. O. Schulz-DuBois

The 34 papers presented at the 5th International Conference on Photon Correlation Techniques include 20 which describe aspects of laser velocimetry and a further 6 concerned with details of the correlation technique. The range of applications is wide and includes a two-dimensional wake, ship wakes, a wing, mixed convection in a cylinder, internal combustion engines, a transonic cascade and turbomachinery. The papers are short and tend to be demonstrative rather than to provide serious attempts to describe fluid-dynamic phenomena. It appears that all papers presented at the Conference are reproduced in the volume and without editing.

The volume is likely to be useful to readers of Heat and Fluid Flow mainly because it reveals the growing range of applications of the photon-correlation technique for the measurement of velocity. It does not provide a balanced view, in that the advantages of the technique, relative to pressure probes, hot-wire, flying hot-wire and pulsed wire anemometry and to alternative methods of processing Doppler and two-spot signals, are not made clear. This is not the fault of the volume but readers should be aware of its narrow perspective, and appraise the possibilities of alternative and probably simpler techniques.

J. H. Whitelaw
Imperial College, London, UK

Published, price DM 80.00, by Springer-Verlag, Heidelberger Platz 3, Postfach, D-1000 Berlin 33, FRG

Books received

Computational Methods for Turbulent Transonic & Viscous Flows, *J. A. Essers,* $49.95, pp 450, Hemisphere Publishing Corporation

Convection in Liquids, *J. K. Platten and J. C. Legros,* DM 180.00 ($71.50 approx), Springer-Verlag

Lehrbuch der Reaktortechnik, $19.90 (DM 48), pp 242, Springer-Verlag

Numerical Modelling in Hydraulics and Water Resources (20th Congress of the International Association for Hydraulic Research) pp 115, IAHR

Fluid Mechanics Measurements, *R. J. Goldstein,* DM 128 ($49.70 approx) pp 630, Springer-Verlag

Energy Storage, £42.00, pp 316, BHRA

Physical Modelling of Multiphase Flow, *ed. H. S. Stephens and C. A. Stapleton,* £30.00, pp 537, BHRA

Cryocoolers—Part 1: Fundamentals, *Graham Walker,* $49.50, pp 365, Plenum Press

Waste Heat: Utilization and Management, *Subrata Sengupta and Samuel S. Lee,* $112.60 (DM 290), pp 1010, Springer-Verlag

Inclusion of a title in this section does not necessarily preclude subsequent review